Applied Catalysis B: Environment and Energy 373 (2025) 125338

Contents lists available at ScienceDirect

Applied Catalysis B: Environment and Energy

journal homepage: www.elsevier.com/locate/apcatb

Reversing the HCl/Cl_2 selectivity for efficient catalytic elimination of dichloromethane by incorporation of Ti^{4+} into CeO_2 lattice

Yunzheng Deng [a,b], Yangyu Shang [a,b], Ting Huang [a,b], Kuangji Li [a,b], Guiying Li [a,b], Yingxin Yu [a,b], Hongli Liu [a,b,*], Taicheng An [a,b]

[a] Guangdong Key Laboratory of Environmental Catalysis and Health Risk Control, Guangdong-Hong Kong-Macao Joint Laboratory for Contaminants Exposure and Health, Institute of Environmental Health and Pollution control, Guangdong University of Technology, Guangzhou 510006, China
[b] Guangdong Engineering Technology Research Center for Photocatalytic Technology Integration and Equipment, Guangdong Basic Research Center of Excellence for Ecological Security and Green Development, School of Environmental Science and Engineering, Guangdong University of Technology, Guangzhou 510006, China

ARTICLE INFO

Keywords:
Chlorinated volatile organic compounds
Metal-organic frameworks
CeO2
Dichloromethane
Catalytic oxidation

ABSTRACT

CeO_2 with impressive redox properties has garnered significant attention in the catalytic removal of hazardous chlorinated volatile organic compounds (CVOCs). Nevertheless, its strong adsorption capacity and pronounced activity in Deacon reaction for dissociated Cl species make it prone to occur chlorine poisoning and generate high reactive Cl_2 rather than ideal HCl, resulting in diminished catalytic stability and increased toxic polychlorinated byproducts. Herein, we proposed the incorporation of Ti^{4+} into the CeO_2 lattice (CeTiO-x, x refers to Ce/Ti molar ratio) through the calcination of bimetallic TiCe-based metal-organic frameworks (MOFs) to effectively oxidize CVOCs. The results demonstrated that such a design could create abundant Ce^{3+}/Ce^{4+} redox pairs stabilized by Ti^{4+} to accelerate substrate thorough degradation into CO_2. Meanwhile, compared to CeO_2, the dissociated Cl species preferentially adsorbed on highly dispersed Ti^{4+} sites instead of Ce^{4+} sites, which allowed for their subsequent release as HCl due to the lower intrinsic reactivity of TiO_2 in Deacon reaction. The cooperation between the reversible Ce^{4+}/Ce^{3+} redox pairs and preferential Cl adsorption on Ti^{4+} sites rendered CeTiO-x catalysts with superior catalytic performance and resistance against chlorine and high humidity. Especially, the optimal CeTiO-10 catalyst achieved > 90 % mineralization rate with complete conversion of dichloromethane at 330 °C during 16 h of continuous oxidation. More importantly, it demonstrated > 95 % selectivity for the desirable HCl, while its counterparts, CeO_2@C and pure CeO_2 catalysts, gave > 90 % Cl_2 selectivity.

1. Introduction

Volatile organic compounds (VOCs) are notorious precursors of ozone and PM2.5, posing a substantial threat to both human health and environmental safety[1–5]. In particular, chlorinated volatile organic compounds (CVOCs) as an intractable type of VOCs have been marked as priority control pollutants in many countries due to their strong intrinsic toxicity, low biodegradability and high photochemical reactivity[4–6]. Consequently, it is highly urgent to develop highly effective technology for CVOCs elimination. Catalytic oxidation with high efficiency and broad applicability is regarded as a promising approach for CVOCs removal, in which CVOCs could be completely oxidized to desirable products of CO_2, H_2O and HCl[4–7]. Compared to non-chlorinated VOCs, the presence of Cl atom in CVOCs makes their oxidation process undergo additional C-Cl bond cleavage and subsequent migration and evolution of the dissociated Cl. During this process, the dissociated Cl is liable to react with intermediates and active sites of catalyst, resulting in catalyst deactivation and the formation of toxic polychlorinated byproducts[4–7]. Therefore, in addition to catalytic activity, enhancing the catalytic stability against chlorine poisoning and synchronously restraining the formation of polychlorinated byproducts have always been the focus and a major challenge.

To overcome the above issues, many attempts have been made to develop effective catalysts, such as V/CeO_2, Ru/CeO_2, MnO_2-$CePO_4/TiO_2$, $Ru/MnCo_3O_x$, V_2O_5-WO_3/TiO_2, H_xPO_4/Ru-CeO_2[8–20]. Thereinto, CeO_2-based catalysts seem to be one of the most promising choices because the facile shift between Ce^{3+} and Ce^{4+} in CeO_2 affords outstanding properties of redox and oxygen storage[15,16]. However,

* Corresponding author at: Guangdong Key Laboratory of Environmental Catalysis and Health Risk Control, Guangdong-Hong Kong-Macao Joint Laboratory for Contaminants Exposure and Health, Institute of Environmental Health and Pollution control, Guangdong University of Technology, Guangzhou 510006, China.
E-mail address: liuhl@gdut.edu.cn (H. Liu).

https://doi.org/10.1016/j.apcatb.2025.125338
Received 28 January 2025; Received in revised form 25 March 2025; Accepted 1 April 2025
Available online 2 April 2025

the dissociated Cl species are often strongly adsorbed on the active sites, which increase the probability of metal chlorination, inducing a rapid deactivation of catalyst and a significant deterioration in catalytic performance[4,5,17–19]. Meanwhile, enhancing redox property of CeO_2-based catalyst is favorable to the deep oxidation of CVOCs into CO_2, but also facilitate oxidation of the adsorbed Cl species into Cl_2 through Deacon reaction[5–7]. High oxidizing ability of the generated Cl_2 usually exacerbates the electrophilic chlorination reaction to produce chlorinated organic byproducts[4–7]. These usually make CeO_2-based catalyst suffer from deactivation and produce more Cl_2 and polychlorinated byproducts. In view of these settings, modulating the adsorption sites for the dissociated Cl species and improving the oxidation ability of CeO_2-based catalyst to refrain from the dissociated Cl species direct contacting with CeO_2 active sites and enable a rapid mineralization of CVOCs are imperative.

Recently, the introduction of transition metal as preferential sites for adsorbing Cl species is a feasible strategy to alleviate the chlorination of the primordial metal active sites[6,19,20]. Whereas it is still necessary to precisely control the combined metal on CeO_2 surface to obtain higher catalyst stability and better catalytic performance. On the other hand, calcination under inert or reducing atmosphere and introduction of dopant ions (such as Ti^{4+}, Zr^{4+}, Ni^{2+}) are effective ways to construct the Ce^{3+} and Ce^{4+} redox pair in CeO_2[21–23]. The unobstructed shifts between Ce^{3+} and Ce^{4+} redox pair were reported to enable activation of the adjacent oxygen atoms and accelerate the electron transfer, thus improving its redox ability and catalytic activity in oxygen evolution reaction, CO oxidation and oxidative depolymerization et al[21–23]. In this regard, the concentration of the Ce^{3+} and Ce^{4+} redox pair is important to its catalytic activity. Moreover, reversible cycle of the Ce^{3+} and Ce^{4+} redox pair is also decisive became Ce^{4+} return to Ce^{3+} is energetically unfavorable[23]. Recently, metal-organic frameworks (MOFs) have become a promising sacrificial template to accurately construct metal oxides through the judicious selection of MOFs precursors and the rational design of pyrolysis conditions due to their periodic structures formed by metal ions and organic ligands[24,25]. Considering that titanium dioxide benefits the adsorption/desorption of Cl and the cleavage of the C–Cl compared to CeO_2[7], we propose the possibility of incorporating Ti^{4+} into CeO_2 lattice via rational calcination of bimetallic TiCe-based MOF to address the above issue of CeO_2-based catalyst in the catalytic oxidation of CVOCs. In this catalyst, the Ti^{4+} sites are expected to preferentially adsorb Cl species and release them in the form of HCl due to its intrinsic inferior activity of Deacon reaction compared to CeO_2. Meanwhile, highly active CeO_2 with abundant Ce^{3+}/Ce^{4+} redox pairs stabilized by Ti^{4+} can promptly oxidate organic intermediates into CO_2 and Cl_2. Their cooperation will decrease the incidence of Cl species reacting with CeO_2 and the generated organic intermediates.

Herein, a typical Ce-MOF, self-assembled by periodic Ce^{4+} and terephthalic acid linkers, was chosen as a host matrix for introducing Ti dopants, rendering bimetallic TiCe-based MOF precursor[26]. Upon calcination under Ar atmosphere at 550 °C and subsequent air treatment at 350 °C, Ti incorporated CeO_2@C samples (denoted CeTiO-x, x refers to the molar ratio of Ce to Ti) with adjustable Ti content were obtained. CeTiO-10 exhibited an optimal catalytic performance with a complete conversion of dichloromethane (DCM) and a mineralization rate of > 90 % at 330 °C. Strikingly, a > 95 % selectivity to HCl was obtained over CeTiO-10, which was completely different from the Cl_2 selectivity (>90 %) of its contrastive CeO_2@C and pure CeO_2 catalysts. Moreover, CeTiO-10 displayed extraordinary catalytic stability and water resistance. Finally, the possible degradation pathway of DCM over CeTiO-10 and the synergistic catalytic mechanism were also proposed.

2. Experimental section

2.1. Catalyst preparation

Ce-MOF and CeTi-MOF-x were synthesized via hydrothermal methods following previous reports with modifications[26]. For the CeO_2@C sample, Ce-MOF precursor was heated at 550 ℃ for 6 h under Ar protection in a tube furnace. After cooling down to room temperature, the solid was further calcined at 350 ℃ for 2 h in air to remove unstable carbon. The CeTiO-x were prepared through a similar procedure to CeO_2@C except that the Ce-MOF was replaced by the CeTi-MOF-x (x refers to the molar ratio of Ce to Ti). As a contrastive catalyst, CeO_2 was synthesized by directly calcining cerium nitrate hexahydrate in a tube furnace at 550 ℃ for 2 h in an air stream.

2.2. Characterization

The morphology of the prepared samples was studied using a transmission electron microscopy (SEM, Talos F200S). The crystal structures of the samples were characterized using powder X-ray diffraction (XRD, Bruker D8 advance). NH_3 temperature-programmed desorption (NH_3-TPD), O_2 temperature-programmed desorption (O_2-TPD), H_2 temperature-programmed reduction (H_2-TPR) were performed on an automatic chemical adsorption instrument (PCA-1200, Builder Electronic Technology Co., Ltd). The H_2 consumption of sample was calculated based on its H_2-TPR peak areas using CuO as calibration standard. The pore structures were obtained by nitrogen adsorption desorption isotherms using BELSORP-max at 77 K. *In-situ* DRIFTS measurements were performed using a ThermoFisher Nicolet IS 10 spectrometer. The amount of Brønsted acid and Lewis acid on CeO_2@C and CeTiO-10 were detected by a Nicolet iS10 spectrometer with pyridine as a probe molecule (Py-FTIR). *In-situ* near ambient pressure X-ray photoelectron spectroscopy (*In-situ* NAP XPS) measurements were conducted using a ThermoFisher Escalab 250Xi instrument. Detailed characterization procedures were provided in the Supporting Information.

2.3. Catalytic performance evaluation and intermediates identification

The DCM catalytic oxidation reactions were performed in a continuous flow fixed-bed quartz microreactor. Before the catalytic reaction, the catalyst was treated at 200 °C in a N_2 stream to remove the adsorbed CO_2 and other impurities. Afterwards, a gaseous mixture consisting of 300 ppm DCM and Air as balance gas was introduced into the reactor at a flow rate of 30 mL/min. The residual DCM, formed organics and CO_2 in the exhaust gas was detected by an online gas chromatograph. For the water resistance test, the procedure was same as the above except the feed gases containing 5.0 vol% water vapor. The concentrations of Cl_2 and HCl in the exhaust gases were determined by using an ion chromatography method and the details were given in the Supporting Information.

3. Results and discussion

3.1. Structural and morphological characterizations of catalysts

As presented in Fig. 1a and Fig. S1, the as-prepared CeTiO-x, CeO_2@C and CeO_2 possessed almost identical characteristic diffraction peaks at 28.6°, 33.1°, 47.5° and 56.3° corresponding to the typical CeO_2 cubic fluorite structure of (JCPDS-ICDD card no. 043–1002). In terms of the five CeTiO-x samples obtained by annealing bimetallic CeTi-MOF with different Ce/Ti molar ratios, the characteristic diffraction peaks of CeO_2 were obviously broadened and weakened than that of CeO_2@C obtained from Ce-MOF, while no diffraction peaks attributable to TiO_2 were detected. These observations were presumably related to the high dispersion of TiO_2 and/or the declined crystallinity resulting from titanium doping into the lattice of CeO_2[27,28].

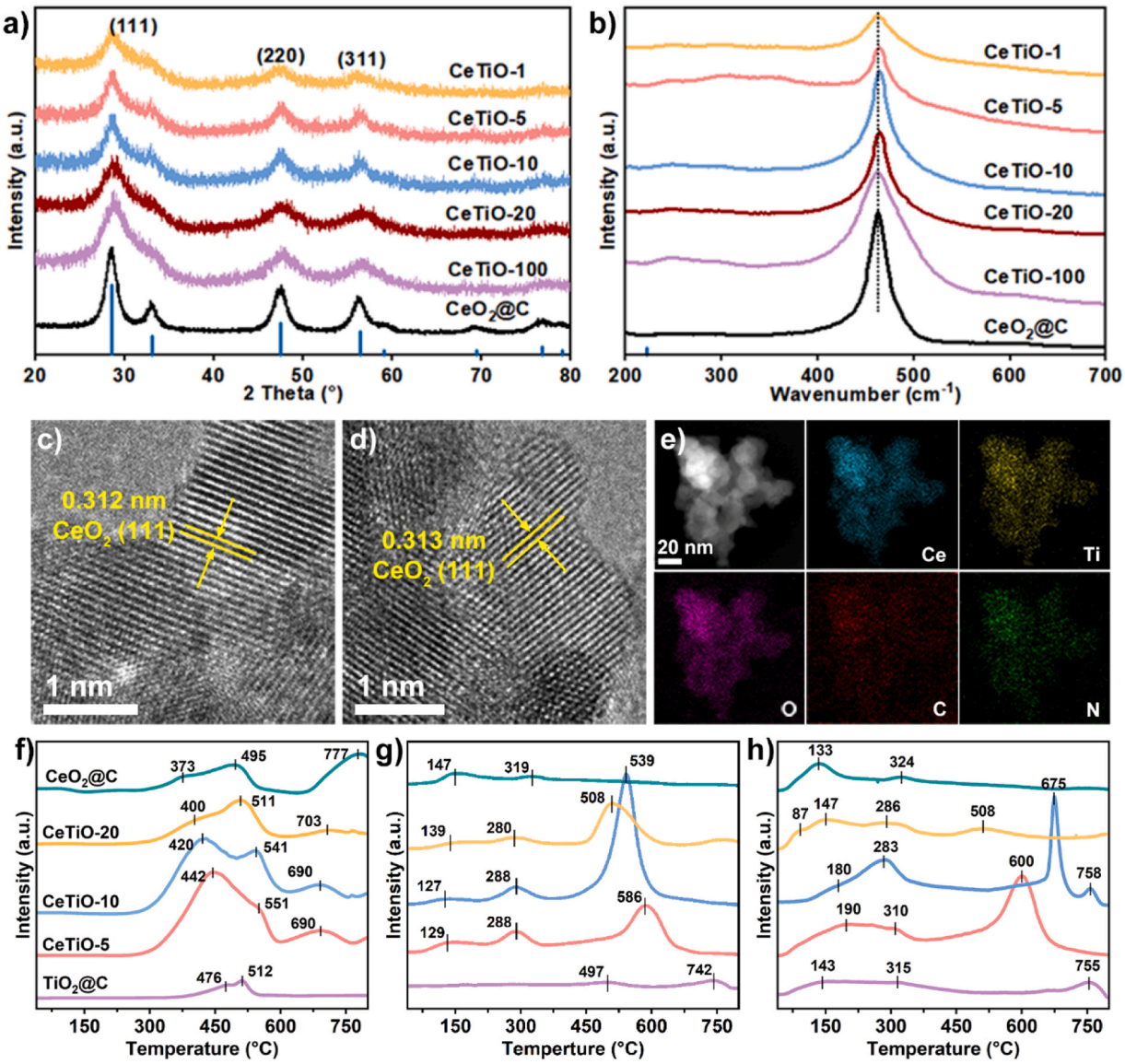

Fig. 1. XRD patterns (a), Raman spectra (b), H_2-TPR (f), O_2-TPD (g) and NH_3-TPD (h) of the synthesized samples. HR-TEM images of CeO_2 (c) and CeTiO-10 (d), and EDS mapping images of CeTiO-10 (e).

To further obtain the impacts of Ti doping on the CeO_2, Raman characterizations of the five CeTiO-x samples and the control CeO_2, CeO_2@C samples were performed. As depicted in Fig. 1b and Fig. S2, CeO_2 prepared by directly calcining $Ce(NO_3)_3{\cdot}6\,H_2O$ and CeO_2@C derived from Ce-MOF displayed a typical F2g mode vibration at around 460 cm^{-1}, which was assigned to the Ce-O symmetric mode vibration of the cubic fluorite structure of CeO_2[29,30]. Moreover, the CeTiO-x samples also exhibited the predominant F2g characteristic peak, further revealing that the Ti doping didn't alter the cubic fluorite structure of CeO_2@C, in consistent with the XRD results (Fig. 1a). Nevertheless, the F2g peaks in the CeTiO-x samples became weaker and broader while their symmetries were worse compared to CeO_2@C and CeO_2. Moreover, these variations were intensified along with the increase of Ti doping amount (Fig. 1b). It should note that a new peak appeared around 600 cm^{-1}, which was attributed to defect-induced (D) mode linked to oxygen vacancies (Fig. S2) [29,30]. In addition, the 2TA (second-order transverse acoustic modes) peak at approximately 260 cm^{-1} in the five CeTiO-x samples was intensified compared to that of CeO_2@C. Wang et al. have found the formation of Pt–O–Ce bond in the Ru/CeO_2 catalysts by Raman spectroscopy[31]. Thus, it is reasonable to tentatively assign these changes and new bands to the formation of Ce–O–Ti bond. Given the difference in atomic radius between Ti (0.145 nm) and Ce (0.183 nm), we inferred that Ti atoms with lower atomic radius replaced some Ce^{4+} cations in the CeTiO-x samples, thereby inducing the lattice shrinkage of CeO_2 and reducing the intensities and symmetries of the XRD and Raman characteristic peaks and inducing oxygen vacancies, as previous reports[30–32].

The TEM images of CeO_2 and CeO_2@C showed that they had the same lattice spacing of 0.313 nm (Fig. 1c and Fig. S3), matching the (111) crystal plane of CeO_2[33]. After incorporating Ti into CeO_2@C, the CeTiO-10 sample still maintained the (111) crystal plane of CeO_2 (Fig. 1d), as observed in XRD. Moreover, the Ti, Ce, C, O and N elements were uniformly distributed across the CeTiO-10 sample (Fig. 1e). The CeO_2@C and CeTiO-10 samples also almost kept the initial morphology of their MOF precursors (Fig. S4-S6). Furthermore, the N_2 adsorption-desorption isotherms of the five CeTiO-x, CeO_2@C and CeO_2 all displayed a characteristic Type IV curve, accompanied by a type H3 hysteresis loop (Fig. S7). Obviously, CeO_2@C displayed a BET surface area of 207 m^2/g, which was significantly larger than that of the five CeTiO-x. Nevertheless, there was no significant difference among their

BET surface areas because they were all extremely low, less than 12 m^2/g.

The surface chemical states and interfacial electron interactions of the as-prepared samples were investigated by X-ray photoelectron spectroscopy (the fresh sample in Fig. S8). For the CeO_2@C, the high-resolution spectrum of Ce 3d can be fitted as eight peaks, corresponding to the Ce^{3+} (blue) and Ce^{4+} species (red)[34], suggesting the co-existence of Ce^{4+} and Ce^{3+} in CeO_2@C sample. This would originate from a partial reduction of Ce^{4+} to Ce^{3+} during the pyrolysis of Ce-MOF precursor. Based on the peak areas of Ce^{4+} and Ce^{3+} species, a $Ce^{3+}/(Ce^{3+}+ Ce^{4+})$ ratio value for CeO_2@C was calculated to be 0.16, which manifested Ce^{4+} as dominant Ce oxidation state in CeO_2@C. When Ti^{4+} was incorporated into Ce-MOF precursor, the resultant CeTiO-10 sample maintained a similar Ce 3d spectrum to that of CeO_2@C. Moreover, its Ti 2p spectrum displayed doublet obvious peaks at 458.16 and 463.52 eV, identified as Ti 2p3/2 and Ti 2p1/2 for Ti^{4+}, further demonstrating the successful incorporation of Ti^{4+} into CeO_2@C. Noticeably, the $Ce^{3+}/(Ce^{3+}+ Ce^{4+})$ ratio in CeTiO-10 improved to 0.23 from 0.16 in CeO_2@C, consistent with the increased oxygen defects as observed by Raman spectroscopy. This increased Ce^{3+} ratio was attributable to a redox process in which the Ti^{4+} incorporated into the CeO_2 lattice during pyrolysis of CeTi-MOF precursor would replace some Ce^{4+} atoms and thereby induced the generation of Ce^{3+} atoms to keep electrostatic balance, as previous reports[35]. It has been reported that the Ce^{3+}/Ce^{4+} redox pair performed an crucial role in promoting various oxidation reactions due to the facile electron transfer through the free electronic communication between Ce^{3+} and Ce^{4+}[21, 22]. Thus the elevated $Ce^{3+}/(Ce^{3+}+ Ce^{4+})$ ratio after the incorporation of Ti^{4+} into CeO_2@C was expected to accelerate the catalytic degradation of DCM.

3.2. Redox property and acidity analyses of catalysts

The redox capacity of the catalysts was further investigated by H_2-TPR. As for CeO_2@C, three H_2 consumption peaks were observed at middle temperatures of 373 and 495 °C, and a high temperature of 777 °C (Fig. 1f), which would result from the reduction of Ce^{4+} to Ce^{3+} on the CeO_2@C surface, and bulk lattice oxygen, respectively[29]. Compared to CeO_2@C, TiO_2@C displayed two higher peak temperatures (476 and 512 °C) at middle temperature range, which would be correlated with the reduction of Ti^{4+} to Ti^{3+}[36]. After the incorporation of Ti into CeO_2, the reduction peaks of the CeTiO-x samples at middle temperatures was obviously shifted to higher temperatures. Moreover, H_2 consumption in the CeTiO-5, CeTiO-10 and CeTiO-20 were estimated to be 0.85, 0.83 and 0.64 mmol/g, which were significantly higher than that for CeO_2@C (Table S1). Given the higher reduction temperature of Ti species than Ce[37,38], we assumed H_2 consumption in the range of 300–600 °C resulted from the reduction of Ce^{4+} to Ce^{3+}, but not the reduction of Ti^{4+} to Ti^{3+}. The reducibility of Ce^{4+} to Ce^{3+} in CeTiO-x increased to 19.67–28.47 % from 8.61 % in CeO_2, which was attributable to the distortion of CeO_2 crystal structure due to the substitution of Ce with Ti, as observed by XRD and Raman results in Figs. 1a and 1b as well as previously reported catalysts[38].

Furthermore, O_2-TPD was conducted to analyze the behavior of surface oxygen species (Fig. 1g). Generally, the O_2 desorption peaks can classified into three categories: the desorption of surface physically adsorbed oxygen below 200 °C, the desorption of surface lattice oxygen in the range of 200–700 °C and the desorption of bulk lattice oxygen above 700 °C[39,40]. As for CeO_2@C, two weak peaks at 147 and 319 °C were observed, indicating the presence of surface physically adsorbed oxygen and surface lattice oxygen, respectively. After incorporating Ti into CeO_2@C, the above two peaks were shifted to lower temperatures compared to CeO_2@C. It is well known that a lower desorption temperature of surface lattice oxygen species leads to a higher concentration of reactive oxygen species due to their excellent mobility, which is essential for enhancing the catalytic oxidation performance[41]. Remarkably, a new strong peak at 586, 539 and 508 °C emerged in CeTiO-5, CeTiO-10 and CeTiO-20, respectively, and CeTiO-10 presented the biggest desorption peak area. It has been reported that the distortion of CeO_2 crystal structure after incorporating the second metal element would result in destabilization of oxide ions due to the variations on Ce-O bond length[42]. Combined with the H_2-TPR results that CeTiO-x exhibited higher reducibility than that for CeO_2@C, it can be concluded that the new strong peak in CeTiO-x should attribute to the desorption of the surface lattice oxygen.

It is widely accepted that the acidic properties of catalyst play a vital role in the adsorption of CVOCs and the subsequent C-Cl dissociation [5–7]. Thus, the surface acidity of CeTiO-x, CeO_2@C and TiO_2@C was characterized by using NH_3-TPD and Py-FTIR. As shown in Fig. 1h, the desorption temperature of NH_3 can be divided into three regions: below 200 °C, 200–500 °C and above 500 °C, which were assigned to weak acidity, medium acidity and strong acidity. Compared to CeO_2@C and TiO_2@C, the CeTiO-x samples exhibited higher intensity in both medium and strong acidity regions, signifying that the introduction of Ti could boost the medium and strong acidic amounts of CeO_2@C. Py-FTIR results showed that CeO_2@C possessed a Lewis acidity of 19.5 μmol g^{-1} and Brønsted acidity of 6.59 μmol g^{-1}. After Ti incorporated into CeO_2, the amount of Lewis acid was slightly decreased to 17.4 μ mol/g, whereas the amount of Brønsted acid was significantly increased to 11.36 μ mol/g (Fig. S9). Based on the H_2-TPR, O_2-TPD and NH_3-TPD results, it could be concluded that the incorporation of Ti significantly improved the amounts of both surface lattice oxygen, and the medium and strong acid as well as Brønsted acid amount on the surface of CeO_2@C.

3.3. DCM catalytic performance and catalyst stability

To verify the promotion effect of Ti incorporating into CeO_2@C catalyst, the catalytic activities of the CeTiO-x catalysts with different Ti loading amounts and their contrastive CeO_2@C and CeO_2 samples were investigated by catalytic degradation of dichloromethane (DCM) in a fixed-bed flow reactor. As illustrated in Fig. 2a and Fig. S10, the $T_{90,\ DCM}$ (the temperature corresponding to the DCM conversion of 90 %) of the investigated catalysts ranked in this order: CeTiO-1 (280 ℃) ≈ CeTiO-5 (280 ℃) < CeTiO-10 (310 ℃) < CeTiO-20 (330 ℃) < CeO_2@C (375 ℃) < CeTiO-100 (400 ℃) ≈ CeO_2 (400 ℃) < TiO_2@C (450 ℃). Intriguingly, the DCM conversion gradually decreased with the increase of the Ti content in the CeTiO-x catalyst, whereas their conversion rates were all higher than CeO_2@C except for CeTiO-100. Nevertheless, the trend of the CO_2 yields over the investigated catalysts didn't correspond to that of their DCM conversion (Fig. 2b). It was obvious that TiO_2@C exhibited the highest $T_{90,\ DCM}$, the lowest mineralization rate. This was attributable to the weakest redox capacity and reactive oxygen mobility of TiO_2@C among the investigated catalysts as revealed by H_2-TPD and O_2-TPD results (Fig. 1f and g), thereby incapacitating the timely oxidation of the intermediates after the cleavage of the C-Cl bond.

For the CeTiO-x catalysts, the mineralization rates at the same reaction time were first gradually improved and then decreased as the Ti content continued to increase, indicating a synergistic interplay between the Ti and CeO_2 active sites in the CeTiO-x samples for improving the DCM degradation activity. Specifically, CeTiO-1 and CeTiO-5 exhibited an exceptional DCM conversion rate of 90 % even at 280 ℃, but their corresponding mineralization rate s were only 41 ± 3.33 % and 39 ± 0.42 %. This phenomenon would be correlated to the accumulation of some unreversible adsorption and/or incomplete degradation of DCM on the catalyst surface[6,43]. Amongst the investigated catalysts, CeTiO-10 presented an optimal catalytic performance with a mineralization rate of 90 % at 330 °C and a DCM conversion of 90 % at 310 °C. Further increasing the Ti content in CeTiO-x brought about decreased DCM conversion and mineralization rate, probably due to the intrinsic low redox capability of TiO_2. It should note that the mineralization rate over CeO_2@C was similar with that of the CeTiO-1 and CeTiO-5, and

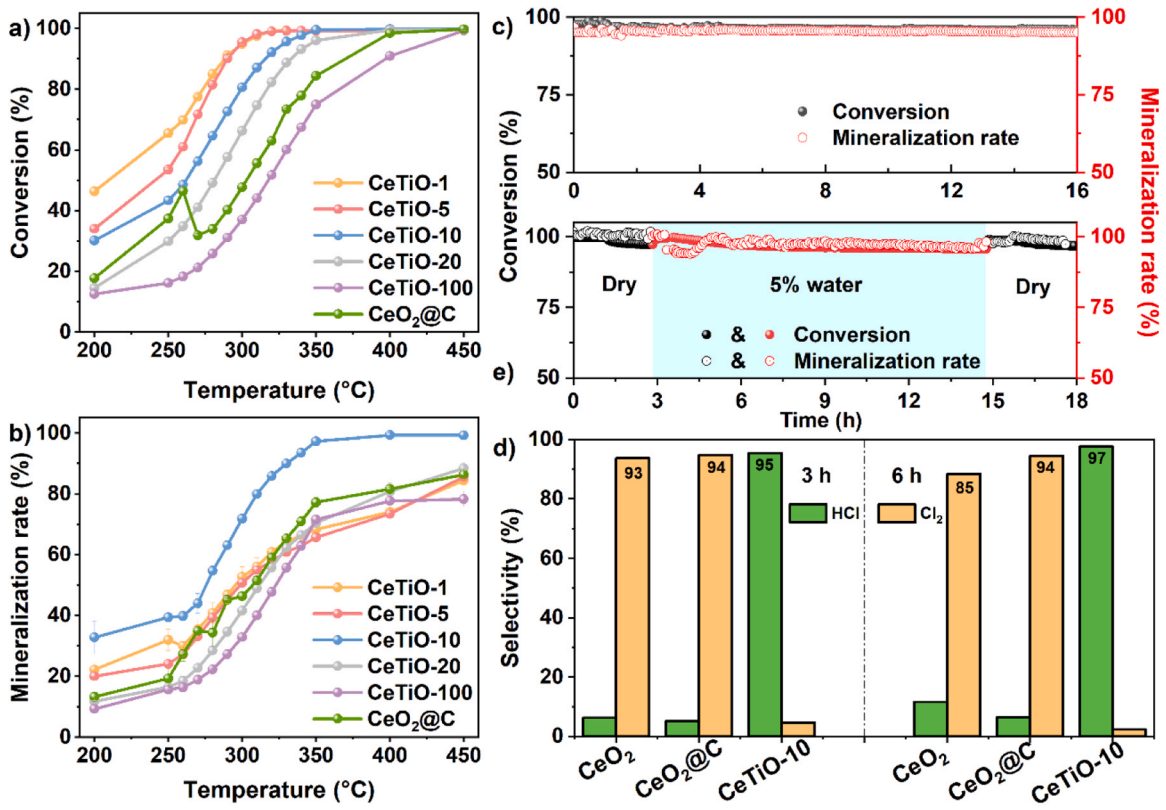

Fig. 2. DCM conversion (a) and corresponding mineralization rate (b) over CeO_2@C and CeTiO-x, catalytic stability of CeTiO-10 for DCM degradation under dry and humid conditions at 330 °C (c), chlorine ions distribution in the outlet gas (d).

slightly higher than that of CeTiO-20 and CeTiO-100. Combining the surface properties of the investigated catalysts (Fig. 1f-h and Fig. S9), it was deduced that the abundant acidic sites and highest redox capacity of CeTiO-10 would accelerate the initial cleavage of C-Cl in DCM and the subsequent deep oxidation of intermediates into final CO_2, responsible for its outstanding DCM degradation performance.

Catalyst deactivation is a pressing and ubiquitous concern in the catalytic oxidation of CVOCs[6]. Thus, long-term stability of the optimal CeTiO-10 catalyst and its contrastive CeO_2@C and CeO_2 catalysts for DCM catalytic oxidation was investigated. As shown in Fig. 2c and Fig. S11, both the DCM conversion and corresponding mineralization rate of the CeTiO-10 catalyst remained unchanged during 16 h of successive reaction, regardless at 330 ℃ or 300 ℃. Moreover, no appreciable changes were observed in the XRD patterns of CeTiO-10 before and after the reaction, illustrating the superior long-term stability of CeTiO-10 for DCM oxidation (Fig. S1). Distinctly different from the CeTiO-10 catalyst, the DCM conversions over the CeO_2@C and CeO_2 catalysts at 330 ℃ began to decrease substantially in the range of 2.0–5.0 h and 1.5–2.5 h, respectively, and then gradually decreased to 66 % and 72 % (Fig. S11), respectively, similar to the commonly observed deactivation in previous reports[41]. Furthermore, the product distributions of inorganic chlorine in the outlet gases after 3 h and 6 h of DCM catalytic reaction were analyzed by ion chromatography. Obviously, HCl was the dominant component with a selectivity exceeding 95 % over the CeTiO-10 catalyst, whereas both the CeO_2@C and CeO_2 catalysts exhibited high selectivity to Cl_2 during DCM oxidation (Fig. 2d). Unfortunately, the possible organic byproducts over CeTiO-10 at 330 ℃ weren't detected by GC-MS. Only trace amount of CH_3Cl could be found even the reaction temperature at 300 ℃ (Fig. S12).

In addition, the water resistance of CeTiO-10 catalyst was examined by introducing 5 vol% water vapors into the feed gases after 3 h of reaction under dry condition. As depicted in Fig. 2c, CeTiO-10 retained DCM conversion to 98 % in humid conditions after 12 h and the corresponding mineralization rate maintained at around 98 % after a slight decrease (< 5 %) within 1 h of test initiation. Once water vapor introduction was stopped, the DCM conversion and mineralization rate slightly returned to their initial levels under dry conditions. The above results distinctly manifested the superior activity, robust stability and water resistance of CeTiO-10 for DCM catalytic degradation, revealing its great potential toward the removal of complicated CVOCs.

3.4. Catalytic degradation mechanism of DCM

To unveil the reasons behind the prominent catalytic activity and stability of CeTiO-10, *in-situ* DRIFTS and *in-situ* NAP XPS studies were further performed to explore the adsorption behaviors, the evolution of intermediates and charge transfer along the DCM catalytic degradation over CeTiO-10. Initially, the temperature-dependent *in-situ* DRIFTS spectra were collected from 30 to 350 °C (Fig. 3, Fig. S13–S16). At 30 °C, stretching vibrations of C-H in DCM molecules were detected at 3062 cm^{-1} and 1270 cm^{-1}, while a bending vibration of C-H can also be found at 2990 cm^{-1} (Fig. 3a) [44]. In addition, their respective absorption peaks gradually intensified over time, indicating the adsorption of DCM on the surface of CeTiO-10. Notably, these peaks associated with DCM disappeared completely above 250 °C, accompanied by the appearance of some new peaks, which was linked to the degradation of DCM and the adsorption of intermediates on the catalyst surface.

At temperatures exceeding 250 °C, a faint new peak around 1455 cm^{-1} could be attributed to the C-H bending vibration of chloromethoxy (CH_2Cl-O-) species, which would result from the dehydrochlorination reaction of DCM over CeTiO-10 [45,46]. Whereas the intensity of this peak was minimal and showed little variation with the reaction temperature and time, signifying a limited accumulation of chloromethoxy over the CeTiO-10 surface throughout the whole DCM oxidation process. At 250 °C, two new peaks at 2933 cm^{-1} and

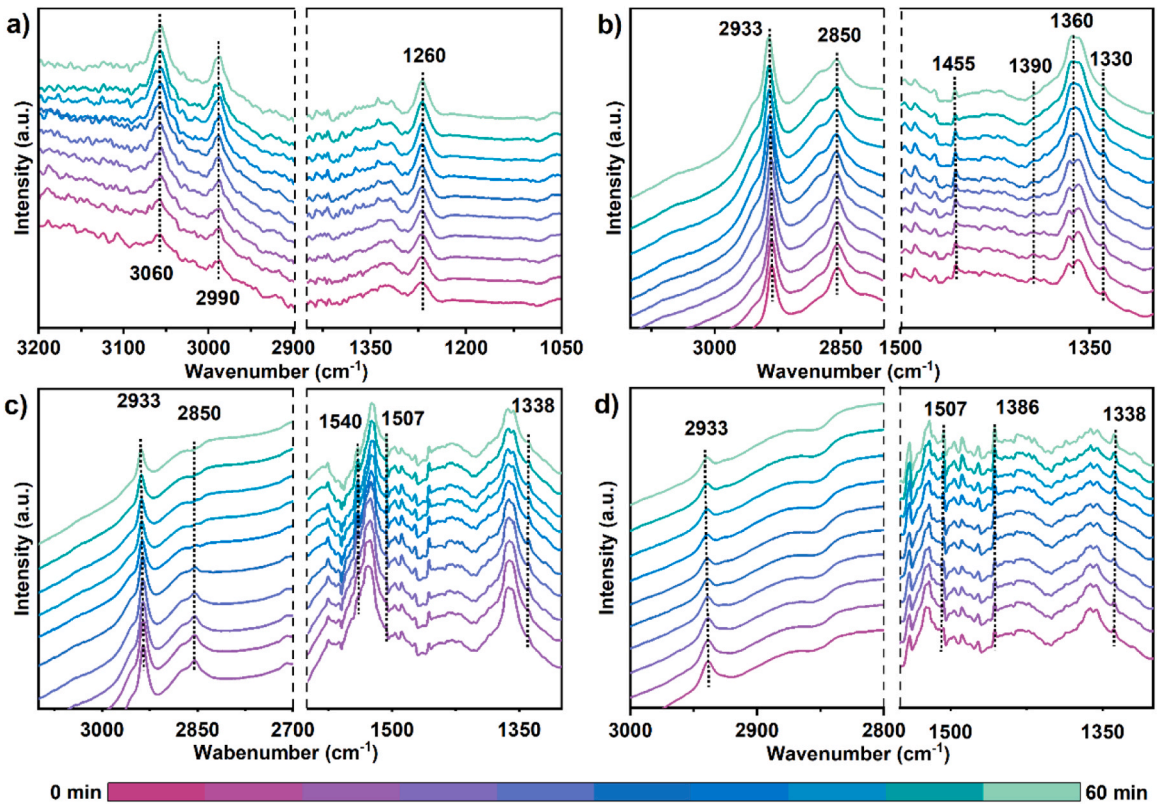

Fig. 3. *In-situ* DRIFT spectra of DCM catalytic oxidation over CeTiO-10 at 30 °C (a), 250 °C (b) 300 °C (c) and 350 °C (d).

2850 cm^{-1} were identified as the asymmetric and symmetric stretching vibrations of C-H in the methoxy group[47]. Additionally, the peaks corresponding to the typical stretching vibration of COO^{-} intermediate can also be found at approximately 1360 cm^{-1} and 1540 cm^{-1}, while vibrations from the -OH in aliphatic alcohol appeared at 1227 cm^{-1}[48, 49]. Moreover, the intensities of the above peaks progressively

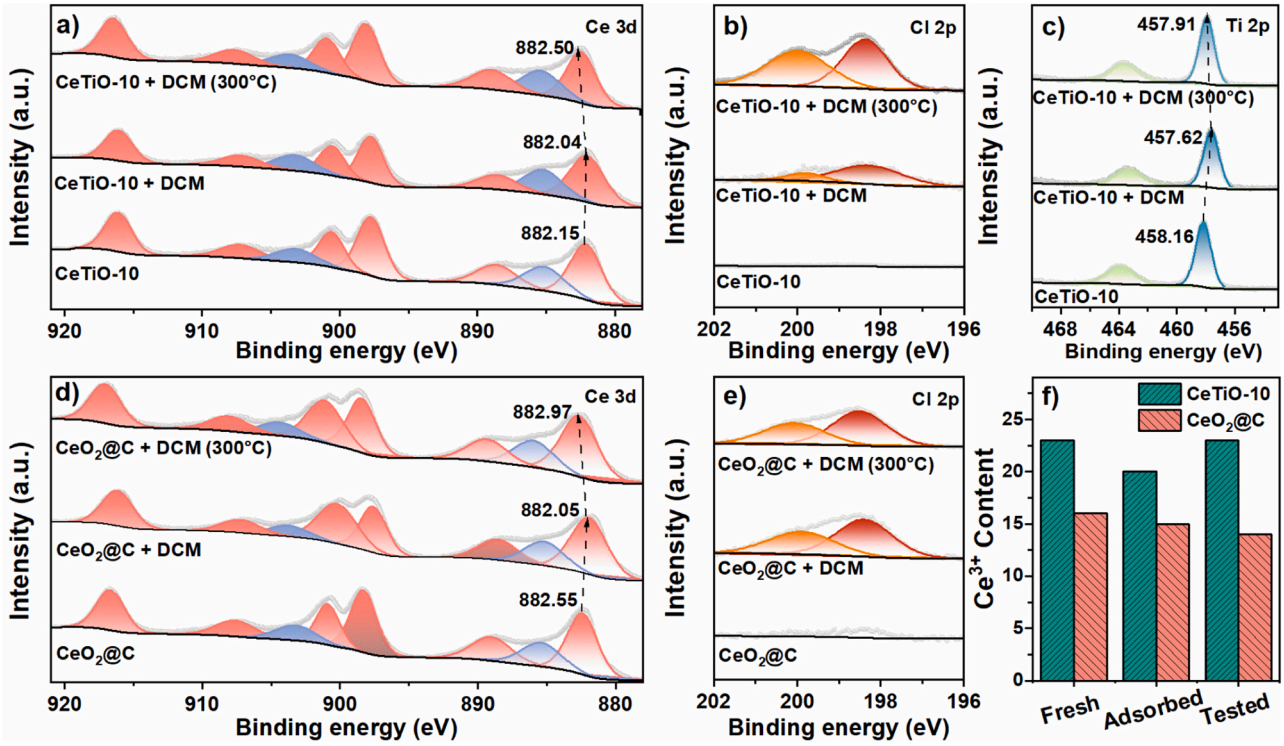

Fig. 4. *In-situ* NAP XPS of Ce 3d (a), Cl 2p (b), Ti 2p (c) for CeTiO-10 and Ce 3d (d), Cl 2p (e) for CeO_2@C. Ce^{3+} content of CeO_2@C and CeTiO-10 catalysts during DCM oxidation (f).

decreased with increasing reaction time. As the temperature rose from 250 to 350 °C, these peaks significantly weakened at the same reaction time and faded away, particularly at 350 °C. These findings suggested that DCM underwent deep oxidation with increasing temperature and time. Combined with the DCM catalytic results (Fig. 2), it can be concluded that DCM was initially dechlorinated and subsequently oxidized to methanol, formaldehyde and formic acid in succession, ultimately transforming into CO_2 and H_2O.

Furthermore, the oxidation processes of DCM over CeTiO-10 and CeO_2@C were tracked by *in-situ* NAP XPS (Fig. 4 and Fig. S17–S23). After introducing gaseous DCM diluted with dry air, two external peaks corresponding to $2p_{3/2}$ and $2p_{1/2}$ of Cl 2p were observed on both CeTiO-10 and CeO_2@C, reflecting the adsorption of DCM on their surface (Fig. 4b and e). For CeO_2@C, six Ce^{4+} peaks displayed an apparent negative shift, whereas a slight positive shift was observed for the two Ce^{3+} peaks compared to that of the fresh CeO_2@C (Fig. 4d), indicating an enhanced electron density around Ce^{4+}. Considering the electron-rich Lewis base nature of Cl in DCM molecule[50], it can be inferred that DCM molecules were adsorbed by Ce^{4+} sites and donated electron to Ce^{4+}. After the temperature increased to 300 °C, the relative content of surface adsorbed oxygen to total oxygen species (Fig. S24) was reduced to 29 % from 36 % in the fresh CeO_2@C. Distinctly different from CeO_2@C, after the adsorption of DCM on CeTiO-10, the negative shift levels of the Ce 2p spectrum were lower than that of the fresh CeTiO-10 (Fig. 4a). Noticeably, the Ti 2p peaks shifted by 0.54 eV toward lower binding energy after the DCM adsorption, which went back to higher binding energies when the temperature elevated to 300 °C (Fig. 4c). These findings implied that DCM molecules would be preferentially adsorbed around Ti sites in CeTiO-10 instead of Ce^{4+} site in CeO_2@C, which could be correlated with stronger adsorption of chlorine on Ti ion than Ce ion[51,52].

It has been demonstrated that abundant oxygen vacancies induced by Ce^{3+} on CeO_2 is conducive to the adsorption of Cl species, yet this also in turn cause deactivation of catalyst[53]. Consequently, the altered preferential adsorption sites for Cl after the incorporation of Ti into CeO_2@C would alleviate the occupation of active sites by Cl species and facilitated reversible cycle of Ce^{3+}/Ce^{4+} redox pairs, thereby affording significantly improved catalytic performance of CeTiO-10 compared to CeO_2@C (Fig. 2). Direct adsorbing Cl species on catalytic sites with high redox ability (such as CeO_2 and RuO_2) was proved to accelerate the Cl_2 formation via Deacon reaction[6,20]. Different from the preferential adsorption of Cl species around Ce^{4+} in CeO_2@C, CeTiO-10 offered abundant Ti sites for Cl adsorption which would avoid direct contact with highly active Ce sites to form Cl_2. Moreover, the inferior oxidation activity of TiO_2@C (Fig. S11) indicated that the Ti sites in CeTiO-10 were incapable of promoting Cl_2 formation at our investigated temperature. It has been reported that Lewis acid sites could promote the breakage of the C-Cl bond and C-H bond, and Brønsted acid sites usually induces the conversion of the adsorbed chlorine ions into HCl by providing H resource[5,6,54]. Therefore, the change in Cl adsorption sites and the increased Brønsted acid amount after incorporation of Ti into CeO_2@C would be responsible for the increase in HCl selectivity from around 10 % for CeO_2@C to > 95 % for CeTiO-10. In addition, after the temperature increased to 300 °C, the Ce^{3+}/ (Ce^{3+}+ Ce^{4+}) ratio of CeO_2@C dropped from 0.16 in the fresh sample to 0.14 (Fig. 4f), while the adsorbed oxygen content also decreased to 29 % from 36 % in the fresh CeO_2@C. By contrast, the Ce^{3+}/ (Ce^{3+}+ Ce^{4+}) ratio in CeTiO-10 remained nearly unchanged before and after DCM catalytic oxidation. These manifested that the incorporated Ti could maintain the Ce^{3+}/ Ce^{4+} redox pairs during DCM catalytic oxidation, in well agreement with the enhanced content of surface adsorbed oxygen and the improved catalytic activity of CeTiO-10 compared to CeO_2@C (Fig. 1g and Fig. 2).

Through the comparison of the catalytic behaviors and surface properties of the investigated catalysts, a possible mechanism for the high effective oxidation of DCM over CeTiO-10 was formulated. The adsorption and activation of DCM first initiated around the Ti sites. Subsequently, a rapid dehydrochlorination step occurred after the C–Cl bond cleavage, accompanying the formation of abundant chloromethoxy species. The increased content of the unobstructed Ce^{4+}/Ce^{3+} redox pair after the incorporation of Ti into CeO_2@C afforded higher oxidation capacity to fleetly oxidate the reaction intermediates to form methanol, formaldehyde and formic acid etc. in succession. Due to the excellent stability of Ce^{4+}/Ce^{3+} redox pair regulated by Ti, the CeTiO-10 sample kept high catalytic activity and ultimately degraded the above intermediates into CO_2 and H_2O. On the other hand, the dissociated chlorine species preferentially adsorbed on Ti sites would avoid direct contact with highly active Ce sites to form Cl_2, thereby selectively converting to HCl with little Cl_2. The interplay of the unobstructed Ce^{4+}/ Ce^{3+} redox pair and the Cl adsorption sites in the CeTiO-10 sample concertedly afford the high DCM deep degradation activity and catalyst stability.

4. Conclusions

In conclusion, CeTiO-x catalysts with different Ti content have been successfully synthesized by controlled calcination of a bimetallic TiCe-based MOF. The stable periodic structures of TiCe-based MOF enabled Ti to uniformly incorporate into the lattice of CeO_2 during the calcination process, thereby inducing abundant Ce^{3+}/Ce^{4+} redox pairs in CeTiO-x. When the obtained CeTiO-x catalysts were employed in DCM catalytic oxidation, an optimal catalytic performance with 90 % CO_2 selectivity and 98 % DCM conversion was achieved over CeTiO-10, which displayed a significant increase compared to that of the undoped CeO_2@C and CeO_2. Meanwhile, CeTiO-10 also offered robust catalytic stability even after 16 h continuous oxidation and excellent water resistance under 5 % vol H_2O. Remarkably, CeTiO-10 manifested a superior HCl selectivity of > 95 %, whereas CeO_2@C and CeO_2 displayed about 90 % Cl_2 selectivity. Mechanism investigations revealed that the reversed HCl selectivity and robust catalytic stability of CeTiO-10 would derive from the preferable Cl adsorption on Ti sites rather than Ce sites. Moreover, the incorporated Ti into CeO_2 lattice facilitated the redox cycle of Ce^{3+}/ Ce^{4+} pairs during DCM catalytic oxidation, which could accelerate the deep oxidation of DCM into CO_2 and H_2O to restrain the generation of polychlorinated byproducts. This work offers a promising strategy to enhance catalytic efficiency and reverse the selectivity to ideal products for CVOCs removal.

Declaration of Competing Interest

The authors declare that they have no known competing financial interests or personal relationships that could have appeared to influence the work reported in this paper.

Acknowledgements

This work was supported by Natural Science Foundation of Guangdong (2022B1515020062), National Natural Science Foundation of China (41991314 and 22076028).

Appendix A. Supporting information

Supplementary data associated with this article can be found in the online version at doi:10.1016/j.apcatb.2025.125338.

Data availability

Data will be made available on request.

References

[1] Y.M. Ji, Q.J. Shi, Y.X. Li, T.C. An, J. Zheng, J.F. Peng, Y.P. Gao, J.Y. Chen, G.Y. Li, Y. Wang, F. Zhang, A.L. Zhang, J.Y. Zhao, M.J. Molina, R.Y. Zhang, Carbenium ion-

mediated oligomerization of methylglyoxal for secondary organic aerosol formation, Proc. Natl. Acad. Sci. U. S. A. 117 (2020) 13294–13299.
[2] J.H. Park, A.H. Goldstein, J. Timkovsky, S. Fares, R. Weber, J. Karlik, R. Holzinger, Active atmosphere-ecosystem exchange of the vast majority of detected volatile organic compounds, Science 341 (2013) 643–647.
[3] Y. Zhang, Y. Wang, R. Xie, H. Huang, M.K.H. Leung, J. Li, D.Y.C. Leung, Photocatalytic oxidation for volatile organic compounds elimination: from fundamental research to practical applications, Environ. Sci. Technol. 56 (2022) 16582–16601.
[4] C. He, J. Cheng, X. Zhang, M. Douthwaite, S. Pattisson, Z. Hao, Recent advances in the catalytic oxidation of volatile organic compounds: a review based on pollutant sorts and sources, Chem. Rev. 119 (2019) 4471–4568.
[5] P. Sun, L. Cheng, S. Gao, X. Weng, X. Dong, Industrial chlorinated organic removal with elimination of secondary pollution: a perspective, J. Phys. Chem. C. 127 (2023) 6610–6618.
[6] F. Lin, Z. Zhang, N. Li, B. Yan, C. He, Z. Hao, G. Chen, How to achieve complete elimination of Cl-VOCs: a critical review on byproducts formation and inhibition strategies during catalytic oxidation, Chem. Eng. J. 404 (2021) 126534.
[7] S.Y. Ding, S.L. Wu, N.J. Fang, Y.H. Chu, P. Wang, Recent advances in chlorinated volatile organic compounds' oxidation over multiple noble metal catalysts: a review based on rational manipulation of redox-acidity balance, Sep. Purif. Technol. 349 (2024) 127859.
[8] S. Wu, X. Lv, X. Hao, J. Chen, H. Jia, Enhancement of mineralization ability and water resistance of vanadium-based catalysts for catalytic oxidation of chlorobenzene by platinum loading, Environ. Sci. Technol. 58 (2024) 15836–15845.
[9] Q. Ying, X. Wang, Y. Liu, Y. Zhang, Z. Wu, Rational design of a novel core–Shell Cu-ZSM-5@Ru/S-1 Tandem catalyst for the catalytic combustion of dichloromethane, ACS EST Eng. 3 (2023) 1013–1021.
[10] X. Yu, J. Deng, Y. Liu, L. Jing, R. Gao, Z. Hou, Z. Zhang, H. Dai, Enhanced water resistance and catalytic performance of Ru/TiO_2 by regulating bronsted acid and oxygen vacancy for the oxidative removal of 1,2-dichloroethane and toluene, Environ. Sci. Technol. 56 (2022) 11739–11749.
[11] M. Tian, Z. Jiang, C. Chen, M. Kosari, X. Li, Y. Jian, Y. Huang, J. Zhang, L. Li, J.-W. Shi, Y. Zhao, C. He, Engineering Ru/$MnCo_3O_x$ for 1,2-dichloroethane benign destruction by strengthening C-Cl cleavage and chlorine desorption: decisive role of H_2O and reaction mechanism, ACS Catal. 12 (2022) 8776–8792.
[12] Q. Dai, K. Shen, W. Deng, Y. Cai, J. Yan, J. Wu, L. Guo, R. Liu, X. Wang, W. Zhan, HCl-tolerant H_xPO_4/RuO_x-CeO_2 catalysts for extremely efficient catalytic elimination of chlorinated VOCs, Environ. Sci. Technol. 55 (2021) 4007–4016.
[13] A. Wang, M. Ding, Y. Cai, L. Wang, Y. Guo, Y. Guo, W. Zhan, Ultra-efficient Ru and Nb Co-modified CeO_2 catalysts for catalytic oxidation of 1,2-dichloroethane, Environ. Sci. Technol. 58 (2024) 20300–20312.
[14] C. Zhang, J. Zhang, Y. Shen, J. He, W. Qu, J. Deng, L. Han, A. Chen, D. Zhang, Synergistic catalytic elimination of NO_x and chlorinated organics: cooperation of acid sites, Environ. Sci. Technol. 56 (2022) 3719–3728.
[15] Q.G. Dai, J.Y. Wu, W. Deng, J.S. Hu, Q.Q. Wu, L.M. Guo, W. Sun, W.C. Zhan, X. Y. Wang, Comparative studies of P/CeO_2 and Ru/CeO_2 catalysts for catalytic combustion of dichloromethane: from effects of H_2O to distribution of chlorinated by-products, Appl. Catal. B Environ. 249 (2019) 9–18.
[16] Q.G. Dai, X.Y. Wang, G.Z. Lu, Low-temperature catalytic combustion of trichloroethylene over cerium oxide and catalyst deactivation, Appl. Catal. B Environ. 81 (2008) 192–202.
[17] Z. El Assal, S. Ojala, S. Pitkäaho, L. Pirault-Roy, B. Darif, J.D. Comparot, M. Bensitel, R.L. Keiski, R. Brahmi, Comparative study on the support properties in the total oxidation of dichloromethane over Pt catalysts, Chem. Eng. J. 313 (2017) 1010–1022.
[18] K. Shen, B. Gao, H.Q. Xia, W. Deng, J.R. Yan, X.H. Guo, Y.L. Guo, X.Y. Wang, W. C. Zhan, Q.G. Dai, Oxy-anionic doping: a new strategy for improving selectivity of Ru/CeO_2 with synergetic versatility and thermal stability for catalytic oxidation of chlorinated volatile organic compounds, Environ. Sci. Technol. 56 (2022) 8854–8863.
[19] R. Gao, M. Zhang, Y. Liu, S. Xie, J. Deng, X. Ke, L. Jing, Z. Hou, X. Zhang, F. Liu, H. Dai, Engineering platinum catalysts via a site-isolation strategy with enhanced chlorine resistance for the elimination of multicomponent VOCs, Environ. Sci. Technol. 56 (2022) 9672–9682.
[20] Y. Long, Q. Meng, M. Chen, X. Luo, Q. Dai, H. Lu, Z. Wu, X. Weng, Selective Ru adsorption on SnO_2/CeO_2 mixed oxides for efficient destruction of multicomponent volatile organic compounds: from laboratory to practical possibility, Environ. Sci. Technol. 56 (2022) 9762–9772.
[21] L. Lei, Y. Wang, Z. Zhang, J. An, F. Wang, Transformations of biomass, its derivatives, and downstream chemicals over ceria catalysts, ACS Catal. 10 (2020) 8788–8814.
[22] J. Yu, X. Du, H. Liu, C. Qiu, R. Yu, S. Li, J. Ren, S. Yang, Mini review on active sites in ce-based electrocatalysts for alkaline water splitting, Energ. Fuel 35 (2021) 19000–19011.
[23] A. Migani, G.N. Vayssilov, S.T. Bromley, F. Illas, K.M. Neyman, Dramatic reduction of the oxygen vacancy formation energy in ceria particles: a possible key to their remarkable reactivity at the nanoscale, J. Mater. Chem. 20 (2010) 10535–10546.
[24] F. Bi, Z. Zhao, Y. Yang, W. Gao, N. Liu, Y. Huang, X. Zhang, Chlorine-coordinated pd single atom enhanced the chlorine resistance for volatile organic compound degradation: mechanism study, Environ. Sci. Technol. 56 (2022) 17321–17330.
[25] A. Hu, Q. Xie, L. Chen, Y. Li, Hierarchically ordered meso-/macroporous MOF-based materials for catalysis and energy applications, EnergyChem 6 (2024) 100137.
[26] S. Payra, S. Ray, R. Sharma, K. Tarafder, P. Mohanty, S. Roy, Photo- and electrocatalytic reduction of CO_2 over metal-organic frameworks and their derived oxides: a correlation of the reaction mechanism with the electronic structure, Inorg. Chem. 61 (2022) 2476–2489.
[27] J.C. Cano-Franco, M. Alvarez-Láinez, Effect of CeO_2 content in morphology and optoelectronic properties of TiO_2-CeO_2 nanoparticles in visible light organic degradation, Mat. Sci. Semicon. Proc. 90 (2019) 190–197.
[28] S.W. Lin, M.H. Tong, Y.X. Chen, R. Chen, H.P. Zhao, X. Jiang, K. Yang, C.Z. Lu, CeO_2/TiO_2 heterojunction nanotube arrays for highly efficient visible-light photoelectrochemical water splitting, ACS Appl. Energy Mater. 6 (2023) 1093–1102.
[29] Y. Shen, J. Deng, X. Hu, X. Chen, H. Yang, D. Cheng, D. Zhang, Expediting toluene combustion by harmonizing the Ce–O strength over co-doped CeZr oxide catalysts, Environ. Sci. Technol. 57 (2023) 1797–1806.
[30] L. Katta, P. Sudarsanam, G. Thrimurthulu, B.M. Reddy, Doped nanosized ceria solid solutions for low temperature soot oxidation: Zirconium versus lanthanum promoters, Appl. Catal. B-Environ. 101 (2010) 101–108.
[31] H. Huang, Q.G. Dai, X.Y. Wang, Morphology effect of Ru/CeO_2 catalysts for the catalytic combustion of chlorobenzene, Appl. Catal. B Environ. 158 (2014) 96–105.
[32] Q.G. Dai, H. Huang, Y. Zhu, W. Deng, S.X. Bai, X.Y. Wang, G.Z. Lu, Catalysis oxidation of 1,2-dichloroethane and ethyl acetate over ceria nanocrystals with well-defined crystal planes, Appl. Catal. B Environ. 117 (2012) 360–368.
[33] B.T. Hu, K.A. Sun, Z.W. Zhuang, Z. Chen, S.J. Liu, W.C. Cheong, C. Chen, M.Z. Hu, X. Cao, J.G. Ma, R.Y. Tu, X.S. Zheng, H. Xiao, X. Chen, Y. Cui, Q. Peng, C. Chen, Y. D. Li, Distinct crystal-facet-dependent behaviors for single-atom palladium-on-ceria catalysts: enhanced stabilization and catalytic properties, Adv. Mater. 34 (2022).
[34] F. Jiang, S.S. Wang, B. Liu, J. Liu, L. Wang, Y. Xiao, Y.B. Xu, X.H. Liu, Insights into the influence of CeO_2 crystal facet on CO_2 hydrogenation to methanol over Pd/CeO_2 catalysts, ACS Catal. 10 (2020) 11493–11509.
[35] D.M. Nguyen, S. Ding, T.T. Nghiem, V.A. Nguyen, E. Mejía, Visible light-driven degradation of trichloroethylene in aqueous phase with vanadium-doped TiO_2 photocatalysts, Sol. RRL 7 (2023) 2200938.
[36] X. Qin, M. Xu, J. Guan, L. Feng, Y. Xu, L. Zheng, M. Wang, J.-W. Zhao, J.-L. Chen, J. Zhang, J. Xie, Z. Yu, R. Zhang, X. Li, X. Liu, J.-X. Liu, J. Zheng, D. Ma, Direct conversion of CO and H_2O to hydrocarbons at atmospheric pressure using a TiO_{2-x}/Ni photothermal catalyst, Nat. Energy 9 (2024) 154–162.
[37] W. Sun, S. Shao, J. Pan, Y. Wang, H. Xia, X. Gao, H. Zhang, Q. Dai, L. Wang, X. Wang, CH_2Cl_2 catalytic oxidation over Ce-Ti-Zr mixed oxide catalysts, Appl. Catal. A Gen. 629 (2022) 118420.
[38] W. Deng, Q. Dai, Y. Lao, B. Shi, X. Wang, Low temperature catalytic combustion of 1,2-dichlorobenzene over CeO_2–TiO_2 mixed oxide catalysts, Appl. Catal. B Environ. 181 (2016) 848–861.
[39] G.Q. Shen, R.R. Zhang, L. Pan, F. Hou, Y.J. Zhao, Z.Y. Shen, W.B. Mi, C.X. Shi, Q. F. Wang, X.W. Zhang, J.J. Zou, Regulating the spin state of Fe^{III} by atomically anchoring on ultrathin titanium dioxide for efficient oxygen evolution electrocatalysis, Angew. Chem. Int. Ed. 59 (2020) 2313–2317.
[40] J. Yang, S.Y. Hu, Y.R. Fang, S. Hoang, L. Li, W.W. Yang, Z.F. Liang, J. Wu, J.P. Hu, W. Xiao, C.Q. Pan, Z. Luo, J. Ding, L.Z. Zhang, Y.B. Guo, Oxygen vacancy promoted o2 activation over perovskite oxide for low-temperature CO oxidation, ACS Catal. 9 (2019) 9751–9763.
[41] X. Lv, S. Wu, S. Shao, D. Yan, W. Xu, H. Jia, H. He, Efficient catalytic elimination of chlorobenzene based on the water vapor-promoting effect within Mn-based catalysts: activity enhancement and polychlorinated byproduct inhibition, Environ. Sci. Technol. 58 (2024) 3985–3996.
[42] G. Dutta, U.V. Waghmare, T. Baidya, M.S. Hegde, K.R. Priolkar, P.R. Sarode, Origin of enhanced reducibility/oxygen storage capacity of $Ce_{1-x}Ti_xO_2$ compared to CeO_2 or TiO_2, Chem. Mater. 18 (2006) 3249–3256.
[43] W.P. Zhang, G.Y. Li, H.L. Liu, J.Y. Chen, S.T. Ma, M.C. Wen, J.J. Kong, T.C. An, Photocatalytic degradation mechanism of gaseous styrene over Au/TiO_2@CNTs: relevance of superficial state with deactivation mechanism, Appl. Catal. B Environ. 272 (2020) 118969.
[44] X.Q. Fei, S. Cao, W.L. Ouyang, Y.X. Wen, H.Q. Wang, Z.B. Wu, A convenient synthesis of core-shell Co_3O_4@ZSM-5 catalysts for the total oxidation of dichloromethane (CH_2Cl_2), Chem. Eng. J. 387 (2020) 123411.
[45] H.J. Zhao, W.L. Han, Z.C. Tang, Tailored design of high-stability $CoMn_{1.5}O_x$@TiO_2 double-wall nanocages derived from Prussian blue analogue for catalytic combustion of o-dichlorobenzene, Appl. Catal. B Environ. 276 (2020) 119133.
[46] Y.Q. Zhao, X.J. Ni, S.J. Ye, Z.G. Gu, Y.X. Li, T. Ngai, A smart route for encapsulating pd nanoparticles into a ZIF-8 hollow microsphere and their superior catalytic properties, Langmuir 36 (2020) 2037–2043.
[47] S. Cao, H.Q. Wang, F.X. Yu, M.P. Shi, S. Chen, X.L. Weng, Y. Liu, Z.B.A. Wu, Catalyst performance and mechanism of catalytic combustion of dichloromethane (CH_2Cl_2) over Ce doped TiO_2, J. Colloid Interf. Sci. 463 (2016) 233–241.
[48] C.Y. Ma, D.H. Wang, W.J. Xue, B.J. Dou, H.L. Wang, Z.P. Hao, Investigation of formaldehyde oxidation over Co_3O_4-CeO_2 and Au/Co_3O_4-CeO_2 catalysts at room temperature: effective removal and determination of reaction mechanism, Environ. Sci. Technol. 45 (2011) 3628–3634.
[49] Y. Wang, A.P. Jia, M.F. Luo, J.Q. Lu, Highly active spinel type $CoCr_2O_4$ catalysts for dichloromethane oxidation, Appl. Catal. B Environ. 165 (2015) 477–486.
[50] Y. Li, H. Zhou, S. Cai, D. Prabhakaran, W. Niu, A. Large, G. Held, R.A. Taylor, X.-P. Wu, S.C.E. Tsang, Electrolyte-assisted polarization leading to enhanced charge separation and solar-to-hydrogen conversion efficiency of seawater splitting, Nat. Catal. 7 (2024) 77–88.
[51] B. Sun, Q. Li, G. Su, B. Meng, M. Wu, Q. Zhang, J. Meng, B. Shi, Insights into chlorobenzene catalytic oxidation over noble metal loading {001}-TiO_2: the role of

$NaBH_4$ and subnanometer Ru undergoing stable $Ru^0 \leftrightarrow Ru^{4+}$ circulation, Environ. Sci. Technol. 56 (2022) 16292–16302.
[52] Z.N. Shi, P. Yang, F. Tao, R.X. Zhou, New insight into the structure of CeO_2-TiO_2 mixed oxides and their excellent catalytic performances for 1,2-dichloroethane oxidation, Chem. Eng. J. 295 (2016) 99–108.
[53] F. Lin, L. Xiang, Z. Zhang, N. Li, B. Yan, C. He, Z. Hao, G. Chen, Comprehensive review on catalytic degradation of Cl-VOCs under the practical application conditions, Crit. Rev. Env. Sci. Tec. 52 (2020) 311–355.
[54] Q.G. Dai, R.H. Xu, H.Q. Xia, B.Y. Qiao, Q. Niu, L. Wang, A.Y. Wang, Y. Guo, Y. L. Guo, W. Wang, W.C. Zhan, Catalytic hydrolysis-oxidation of halogenated methanes over phase- and defect-engineered $CePO_4$: halogenated byproduct-free and stable elimination, Environ. Sci. Technol. 58 (2024) 13562–13573.